# Motion of three inelastic particles on a ring

Elizabeth Grossman and Muhittin Mungan
*University of Chicago, The James Franck Institute, 5640 South Ellis Avenue, Chicago, Illinois 60637*
(Received 6 September 1995)

In a previous paper [P. Constantin, E. Grossman, and M. Mungan, Physica D **83**, 409 (1995)], we have studied in detail the dynamics of three inelastically colliding particles moving on an infinite line. The present paper addresses the effect of boundary conditions by investigating both analytically and numerically the dynamics of three particles confined to a ring. Using the methods developed in [P. Constantin, E. Grossman, and M. Mungan, Physica D **83**, 409 (1995)], we reformulate the dynamics as a billiard in an equilateral triangle with nonspecular reflections laws. There are three sharply distinct regimes: (i) perfectly elastic collisions, (ii) slightly inelastic collisions, and (iii) strongly inelastic collisions. In particular, in the limit of the inelasticity going to zero, the asymptotic motion in case (ii) does not reduce to case (i), i.e., perfectly elastic motion is a singular limit. For motion on the line in the strongly inelastic regime, particles can either cluster, undergoing infinitely many collisions while their relative separation goes to zero (inelastic collapse), or they can separate after a finite number of collisions (escape). The confinement to a circle, while greatly enhancing the occurrence of clustering, does not completely eliminate the existence of other asymptotic states. In fact, there exists a fractal set of initial conditions for which collisions proceed indefinitely without clustering. [S1063-651X(96)01006-9]

PACS number(s): 46.10.+z, 03.20.+i, 05.45.+b, 47.53.+n

## I. INTRODUCTION

Inelastic collisions of particles on a line or in the plane have been studied with increased interest over the past several years [1–5]. It has been observed that due to the energy loss in successive collisions, these systems can evolve into a clustering state in which the number of collisions per unit time increases without bound, while the mean free path goes to zero. This phenomenon has been termed ''inelastic collapse'' [3] and is qualitatively akin to the behavior of one inelastic ball bouncing repeatedly off the ground.

The occurrence of inelastic collapse on a line depends on the number of particles present and on the coefficient of restitution $r$. Specifically, for three particles on a line it has been shown [1–3,6] that collapse can occur when $r$ is below a critical value $r_{\rm cr}=7-4\sqrt{3}$. In a previous work [1], we have analyzed the dynamics of this system, both above and below the critical $r$ value. The aim of this paper is to investigate how the dynamics is changed when the system is confined to move on a ring, i.e., when periodic boundary conditions are imposed.

In Sec. I A, we formulate the dynamics of three particles on a line in a way suitable for extension to the ring. For motion on the line, the dynamics is equivalent to a billiard in a semi-infinite wedge, while confining the system to a circular configuration generates a billiard in an equilateral triangle. In either case, the reflections are not specular.

In Sec. II we examine the quasielastic regime ($r>r_{\rm cr}$). Section II A provides an overview of the types of behavior observed in this range of $r$ values. Secs. II B and II C concentrate on specific cases of interest. (i) The completely elastic case $r=1$: Here, the reflection laws turn out to be specular, and we have a conventional billiard in an equilateral triangle. (ii) The nearly elastic case, $r=1-\epsilon$ (in particular, the behavior as $\epsilon\to 0$): Numerical findings suggest that the asymptotic dynamics for these $r$ is governed by a strange attractor.

The most immediate consequence of imposing periodic boundary conditions on the three particles is the elimination of escape; all initial conditions give rise to an infinite sequence of collisions. Section III examines the strongly inelastic region ($r\leqslant r_{\rm cr}$). It turns out that almost all initial conditions result in inelastic collapse, but nonetheless there does exist a fractal set of initial data that generates a sequence of infinite but non-collapsing trajectories.

### A. A review of inelastic collisions and motion on a line

In [1], we obtained an analytic description of the dynamics of three inelastically colliding particles confined to move on an infinite line. The inelasticity is parameterized by the coefficient of restitution $r$ as

$$v_2'-v_1'=-r(v_2-v_1), \tag{1.1}$$

where $v_{1,2}$ and $v_{1,2}'$ are the velocities before and after a binary collision. The completely elastic case occurs when $r=1$ and energy is conserved, whereas at $r=0$, the collision is completely inelastic and the particles emerge stuck together. Equation (1.1) and conservation of momentum allow us to express the velocities after a binary collision in terms of those before

$$\begin{pmatrix} v_1' \\ v_2' \end{pmatrix} = \begin{pmatrix} (1-r)/2 & (1+r)/2 \\ (1+r)/2 & (1-r)/2 \end{pmatrix} \begin{pmatrix} v_1 \\ v_2 \end{pmatrix}, \tag{1.2}$$

where we have assumed that the particles have equal masses.

 

When viewed in the plane of relative separations ($x_{12}$ and $x_{23}$) the dynamics of three inelastically colliding particles is equivalent to the motion of a nonoptical billiard within a semi-infinite wedge (see Fig. 1). Collisions of the particles correspond to reflections at the boundaries of the wedge, which represent the lines $x_{12}=0$ and $x_{23}=0$. Between these walls, the trajectory moves along a straight line whose generalized slope $s_n$ is defined as

$$s_n=-\frac{d_{n+1}}{d_n}=\begin{cases}\dfrac{v_3-v_2}{v_2-v_1} & \text{for trajectories emerging from the } x_{23}=0 \text{ axis}\\[2ex] \dfrac{v_1-v_2}{v_2-v_3} & \text{for trajectories emerging from the } x_{12}=0 \text{ axis.}\end{cases} \tag{1.3}$$

Using expression (1.2) for the change in the velocities due to a binary collision, we obtain the mapping $f_1: s_n \to s_{n+1}$ that describes the change in the slope upon reflection

$$s_{n+1}=-\frac{r}{b+s_n}\equiv f_1(s_n), \tag{1.4}$$

where $b=1/2(1+r)$.

The initial data of the system is now reduced to a distance $d_0\in[-\infty,\infty]$ and a slope $s_0\in[-\infty,\infty]$. The latter, via (1.4), generates a sequence of slopes, $s_i<0$, $i=1,2,3,\ldots$, that terminates with the smallest $n$ such that $s_n>0$. Such a slope corresponds to a trajectory that is moving away from both the $x_{12}$ and the $x_{23}$ axes, and hence no further collisions can occur. Depending on $r$, we see two distinct regimes [1–3]:

(I) *The strongly inelastic regime*, $r\leqslant r_{cr}=7-4\sqrt{3}$: For this range of $r$ values, the mapping (1.4) has two real fixed points $s_-^*<s_+^*<0$; $s_-^*$ is unstable, while $s_+^*$ is stable, with a basin of attraction consisting of all initial slopes $s_0>s_-^*$. Thus the sequence of slopes generated by such an $s_0$ approaches the fixed point $s_+^*$ and the series does not terminate. In the billiard picture, such an infinite sequence corresponds to a trajectory zigzagging into the origin, while the corresponding motion in configuration space is such that the relative separations of the particles go to zero. We refer to these states as asymptotic bound states. For $s_0<s_-^*$, the sequence is not drawn to the fixed point; eventually the slope assumes a non-negative value and the series terminates, indicating that the particles are all moving away from each other. We call such states asymptotic free states.

(II) *The quasielastic regime* $r>r_{cr}$: In this regime the recursion (1.4) has no real fixed points and any $s_0\in[-\infty,\infty]$ generates a sequence that terminates after a finite number of reflections. Thus in this regime we have only asymptotic free states.

### B. The equations of motion on the circle

By an extension of the above method, the dynamics of three particles on a ring can be considered as a billiard in an equilateral triangle. If the circle has unit circumference, the triangle has edges of length one, its sides representing the lines $x_{12}=0$, $x_{23}=0$ and $x_{31}=0$ (see Fig. 2). The vertices are the intersections of these lines and hence correspond to triple collisions. Each vertex is uniquely labeled by the middle particle in such a grouping.

Consider a pair of successive collisions. This pair will have a middle particle, one which is involved in both colli-

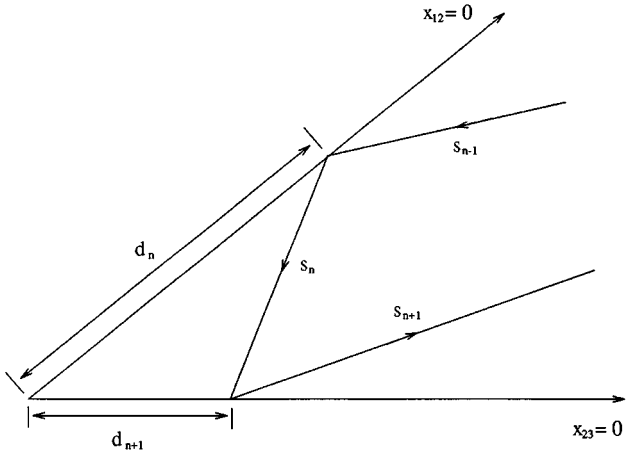


FIG. 1. The variable conventions for a billiard moving in a semi-infinite wedge. This system is equivalent to three particles moving on an infinite line with relative separations $x_{12}$ and $x_{23}$.

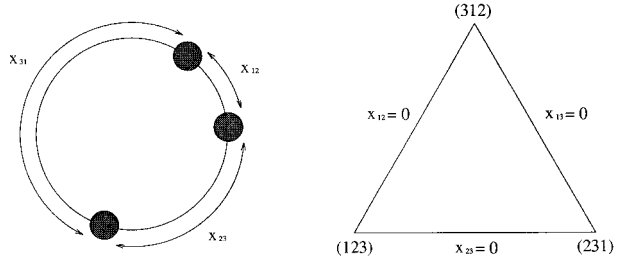


FIG. 2. (a) The configuration space. (b) The corresponding billiard. Collisions between two particles correspond to reflections, and hence at each side of the triangle, one of the relative separations is zero. The vertices are the three possible cyclical arrangements of the particles when touching. Each vertex is uniquely labeled by the middle particle.

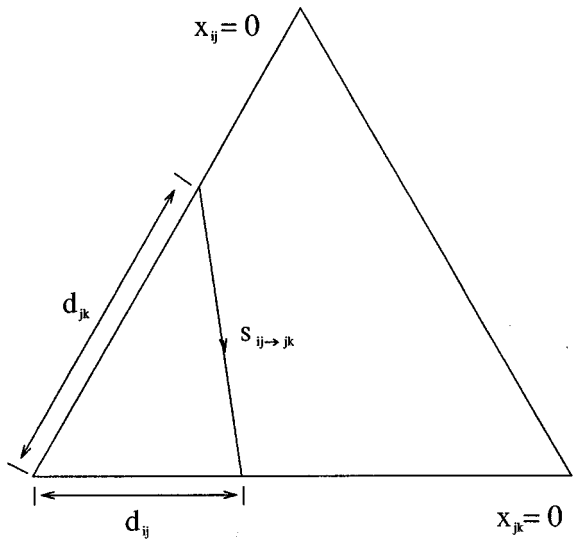


FIG. 3. The variable conventions for a billiard trajectory in the equilateral triangle.

sions; label it $j$. There will also be two outer particles $i$ and $k$ such that the first particle $j$ collides with $i$, then with $k$ (of course $i \neq j \neq k$). Denote the distance between particles $j$ and $k$ ($i$ and $j$) at the time of the first (second) collision by $d_{jk}$ ($d_{ij}$). Associate with this pair of successive collisions a directed line segment in the billiard $\overrightarrow{d_{jk}d_{ij}}$ as shown in Fig. 3. Proceeding in this manner, the successive collisions on the circle generate a billiard trajectory within the triangle. Furthermore, each line segment $\overrightarrow{d_{jk}d_{ij}}$ has a generalized slope, $s_{ij\to jk}$, given by

$$s_{ij\to jk} = -\frac{d_{ij}}{d_{jk}}, \tag{1.5}$$

which is, again, related to the velocities of the particles between the two collisions [cf. Eq. (1.3)]:

$$s_{ij\to jk} = \frac{v_j - v_i}{v_k - v_j}. \tag{1.6}$$

Thus the line segment $\overrightarrow{d_{jk}d_{ij}}$ is well determined by the point of emergence $d_{jk}$ and the generalized slope $s_{ij\to jk}$.

As long as the collisions proceed in a way that $j$ remains the middle particle, the particles do not experience the boundedness of their configuration space and hence the dynamics is identical to that occurring on the infinite straight line. This situation breaks down when the outer particles collide with each other. At this point, one of these outer particles becomes the middle particle. In the billiard this corresponds to a trajectory changing corners. Therefore, given a line segment described by the pair $(s_n, d_n)$, there are two distinct possibilities for the subsequent segment $(s_{n+1}, d_{n+1})$ (see Fig. 4); given in terms of $(s_n, d_n)$, these are as follows. For case I:

$$\begin{aligned} s_{n+1} &= f_1(s_n) = -r/(b + s_n) \\ d_{n+1} &= -d_n s_n . \end{aligned} \tag{1.7a}$$

For case II:

$$\begin{aligned} s_{n+1} &= f_1(-1 - s_n) = -r/(b - 1 - s_n) \\ d_{n+1} &= 1 + d_n s_n . \end{aligned} \tag{1.7b}$$

In order to derive the recursion for the slope in (1.7b), note the following. When both the incident and reflecting slope are expressed with respect to the same corner, the reflection law is given by $f_1(s)$, as discussed in Sec. I A and seen in case I. For case II, where the trajectory is changing corners, we can still make use of $f_1(s)$ if the incident slope is re-expressed in terms of the new corner. This re-expression corresponds to a permutation of the velocities in (1.6). One finds that $s_n \to -1 - s_n$, and thus $s_{n+1} = f_1(-1 - s_n)$ for case II.

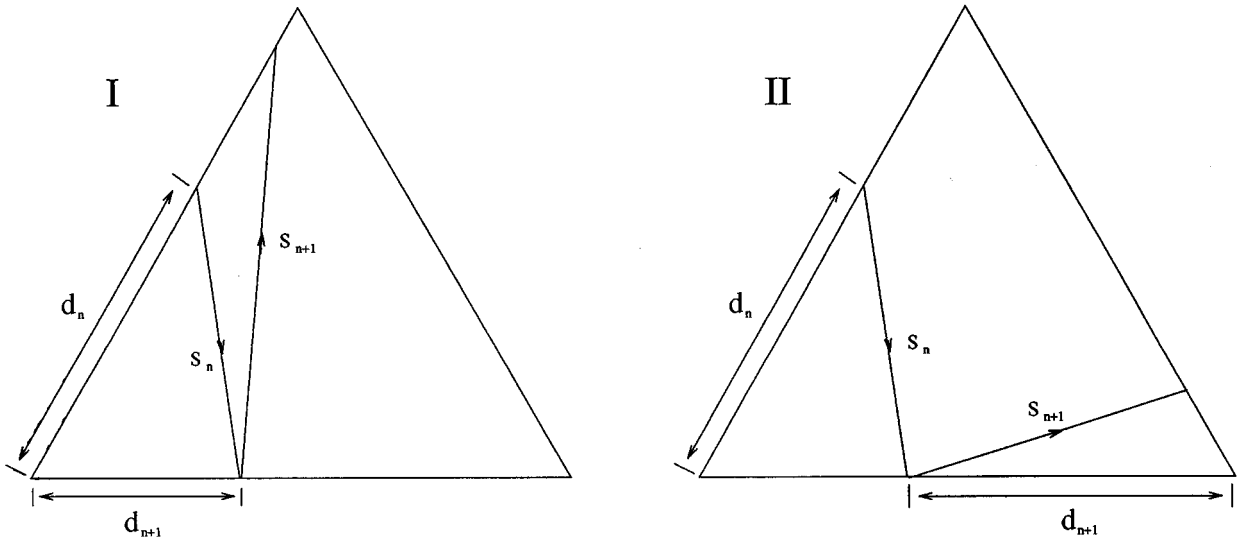


FIG. 4. Given a segment $(s_n, d_n)$, there are two possibilities for the next type of step. For type I, the trajectory remains in the same corner (the middle particle does not change), while for type II, the billiard shifts to a different corner (there is a new middle particle).

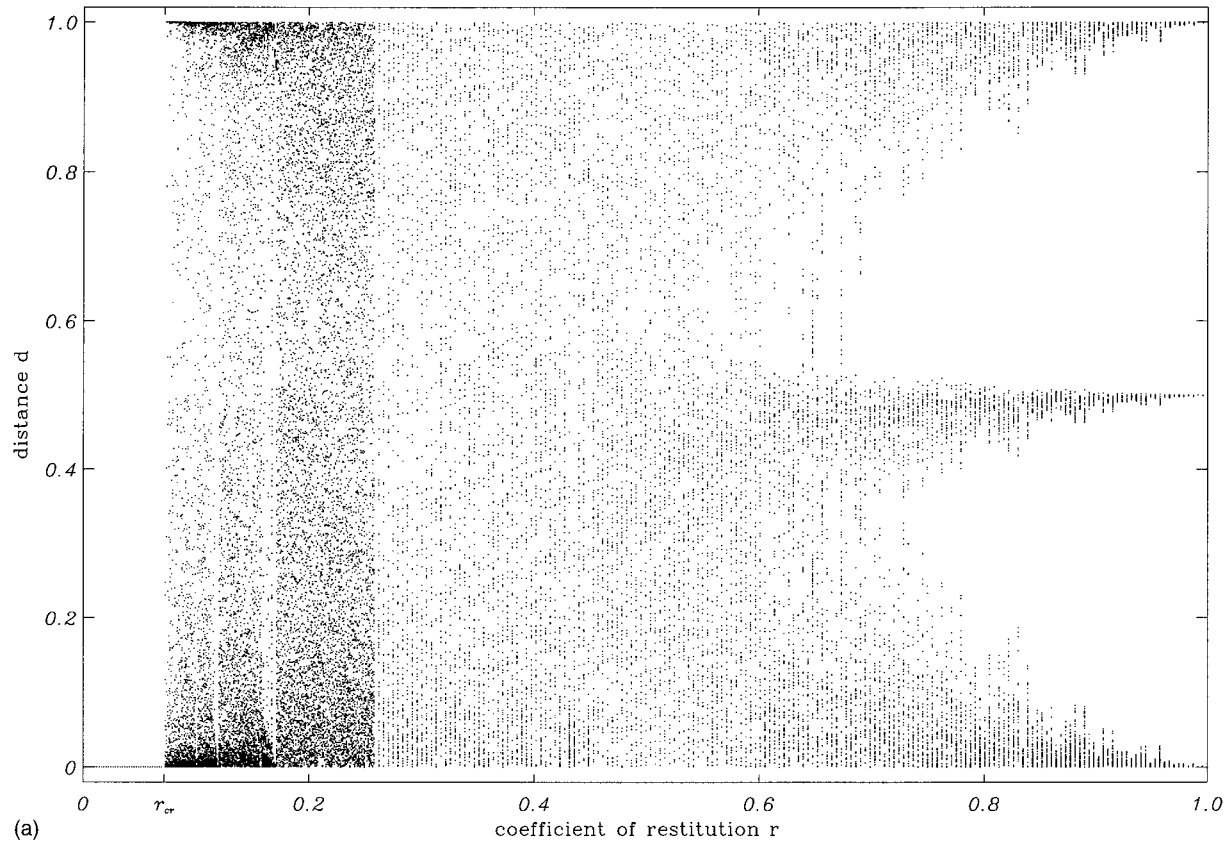


FIG. 5. Long-term behavior of the billiard as a function of $r$. For a fixed $r$, the trajectory is allowed to evolve for $2\times10^6$ bounces from random initial conditions and the last 200 distances $d$ are plotted versus $r$ on the vertical axis. (a) The full range of $r$ values. Notice that for $r\leqslant r_{\rm cr}$ collapse always occurs in the simulations. Thus the distances all go to zero at large times (see Sec. III). (b) Replot of (a) for $r>r_{\rm cr}$, the horizontal axis has been rescaled to highlight the appearance of the pseudoperiodic windows as $r\to r_{\rm cr}$. (c) Plot of the last 200 slopes. The vertical axis is actually $\tan^{-1}(s)$.

Given a segment $(s_n,d_n)$, the question whether to proceed via I or II is determined by assuming that I is applied twice and checking to see if $d_{n+2}$ is a permissible distance, i.e., between zero and one. In other words,

$$z_n=-d_{n+1}s_{n+1}=-(-d_ns_n)[-r/(b+s_n)] \qquad (1.8)$$

and if $z_n\in(0,1)$, the evolution proceeds via I, indicating that the corner has not changed. Conversely, if $z_n\notin[0,1]$, there is a change of corner, and the system evolves under II.

Thus the two-dimensional recursion for the motion of three inelastically colliding particles on a ring (or one nonspecular billiard in an equilateral triangle) is given by

$$\begin{pmatrix} s_{n+1} \\ d_{n+1} \end{pmatrix}=\begin{cases} f_{\rm I}\begin{pmatrix} s_n \\ d_n \end{pmatrix}=\begin{pmatrix} -r/(b+s_n) \\ -d_ns_n \end{pmatrix} & \text{if } 0<z_n<1 \\ f_{\rm II}\begin{pmatrix} s_n \\ d_n \end{pmatrix}=\begin{pmatrix} -r/(b-1-s_n) \\ 1+d_ns_n \end{pmatrix} & \text{otherwise} \end{cases} \qquad (1.9)$$

and the initial data for this recursion is a pair

$$(s_0,d_0) \text{ such that } s_0<0, d_0\in(0,1),$$

$$\text{and } d_1=-s_0d_0\in(0,1);$$

in particular, this guarantees that $s_n<0$ for all $n$. Note that we exclude trajectories that are incident on or emergent from the corners. The above description does not distinguish among the three corners of the billiard, which is natural as the particles themselves are indistinguishable.

## II. THE QUASIELASTIC REGIME: $r>r_{\rm cr}$

### A. The quasielastic regime in general $(1>r>r_{\rm cr})$

Simulations of three particles confined to a ring indicate the existence of two types of long-term behavior in the quasielastic regime—full exploration of phase space or some sort of pseudoperiodic orbit. In the billiard picture, the former corresponds to a trajectory that ''fills'' the triangle, with no *a priori* limits on the possible $s$ and $d$ values. The latter case appears as a trajectory that visits only certain parts of the triangle, i.e., certain finite ranges of $s$ and $d$ values. Numerically, which type of asymptotic trajectory occurs seems to depend only on $r$, not on initial conditions.

Figure 5(a) visualizes this dependence. The horizontal axis is the coefficient of restitution. For each $r\in(0,1)$, the system evolves from the random initial conditions for $2\times10^6$ bounces. The $d$ values for the last 200 reflections are then plotted against $r$. If $r$ is such that the trajectory fills the triangle, $d$ is seen to appear anywhere within its permissible domain, (0,1). If, however, the $r$ value produces a pseudoperiodic orbit, $d$ is observed to be limited to select regions of this domain.

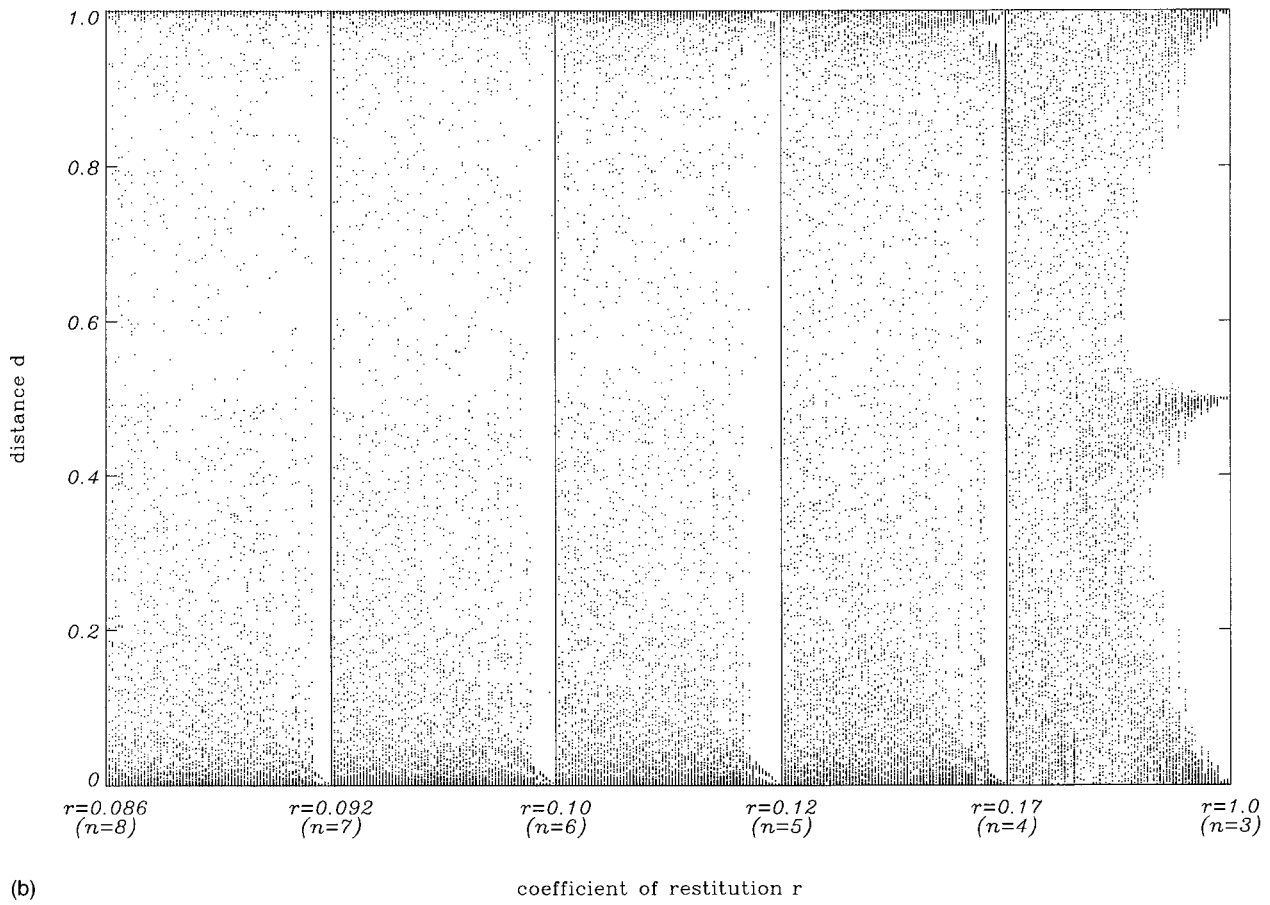


FIG. 5 (*Continued*).

For $r \leqslant r_{\mathrm{cr}}$, all the computer generated initial conditions result in collapse ($d \to 0$). For $r > r_{\mathrm{cr}}$, there seems to be a large pseudoperiodic window near $r=1$, another at $r \sim 0.17$, and there are more at lower $r$ values greater than $r_{\mathrm{cr}}$. In fact, Fig. 5(b) shows a section of Fig. 5(a) rescaled to highlight the positions of some of these windows. Figure 5(c) is a plot equivalent to Fig. 5(b), but instead of $d$ on the vertical axis, $\tan^{-1}(s)$ has been plotted. It is clear that the period of these special orbits increases as $r$ decreases. For all the windows (except that near $r=1$), $d$ is limited to values that are nearly one or nearly zero, i.e., all the reflections occur close to the corners of the triangle. If we examine the trajectories from the window at $r \sim 0.17$, we find that they consist of five bounces in a corner, the last of which moves the trajectory to another corner, where there are again five bounces. The trajectories then return to the original corner and the pattern repeats. The position along the walls (and hence the slopes) of the reflections in each corner vary slightly from cycle to cycle, but stay within a confined range. This is what we mean by a pseudoperiodic orbit. This pattern turns out to be typical of the trajectories in all the windows. For example, near $r=0.12$, the trajectories always undergo six reflections per corner and this time visit all three corners of the triangle before repeating. We can summarize our computational understanding of these pseudoperiodic trajectories as follows: label the windows by $n$, where near $r=1$ is $n=3$, near $r=0.17$ is $n=4$, near $r=0.12$ is $n=5$, etc.; then the trajectories in the $n$th window always have $n+1$ reflections per corner; if $n$ is even the trajectory alternates between two corners; if it is odd, it rotates among all three. Note that the first window ($n=3$) does not quite conform to this pattern.

As discussed above, the motion of the billiard within a corner is equivalent to the motion of three particles on a line; the middle particle remains the same so the constraint of the circular geometry is not felt. On a line, for each $r > r_{\mathrm{cr}}$ there exists an upper bound $n_{\max}(r)$ on the number of collisions that can occur before escape [1]. On the circle, this limit corresponds to the maximum number of collisions that can occur within a corner. The function $n_{\max}(r)$ can be used to find $r_n$, such that if $r \in [r_{n+1}, r_n)$, $n+1$ is the maximum number of collisions that may occur [7]

$$\frac{16 r_n}{(1+r_n)^2} = 1 + \tan^2\left(\frac{\pi}{n}\right) \qquad n = 3,4,5,\ldots \,. \tag{2.1}$$

Thus, for example, the trajectories that occur near $r \sim 0.17$ could only exist for $r < r_4$. In fact, we find numerically that the upper boundaries of the windows are given by these $r_n$: $r$ values just below $r_n$ produce pseudoperiodic orbits with $n+1$ reflections per corner while $r$ values just above $r_n$ produce trajectories that fill the phase space. The linking of these pseudoperiodic regions to a well understood sequence of $r$ values leads us to believe that there are a countably infinite number of such windows in the range $r \in (r_{\mathrm{cr}}, 1)$.

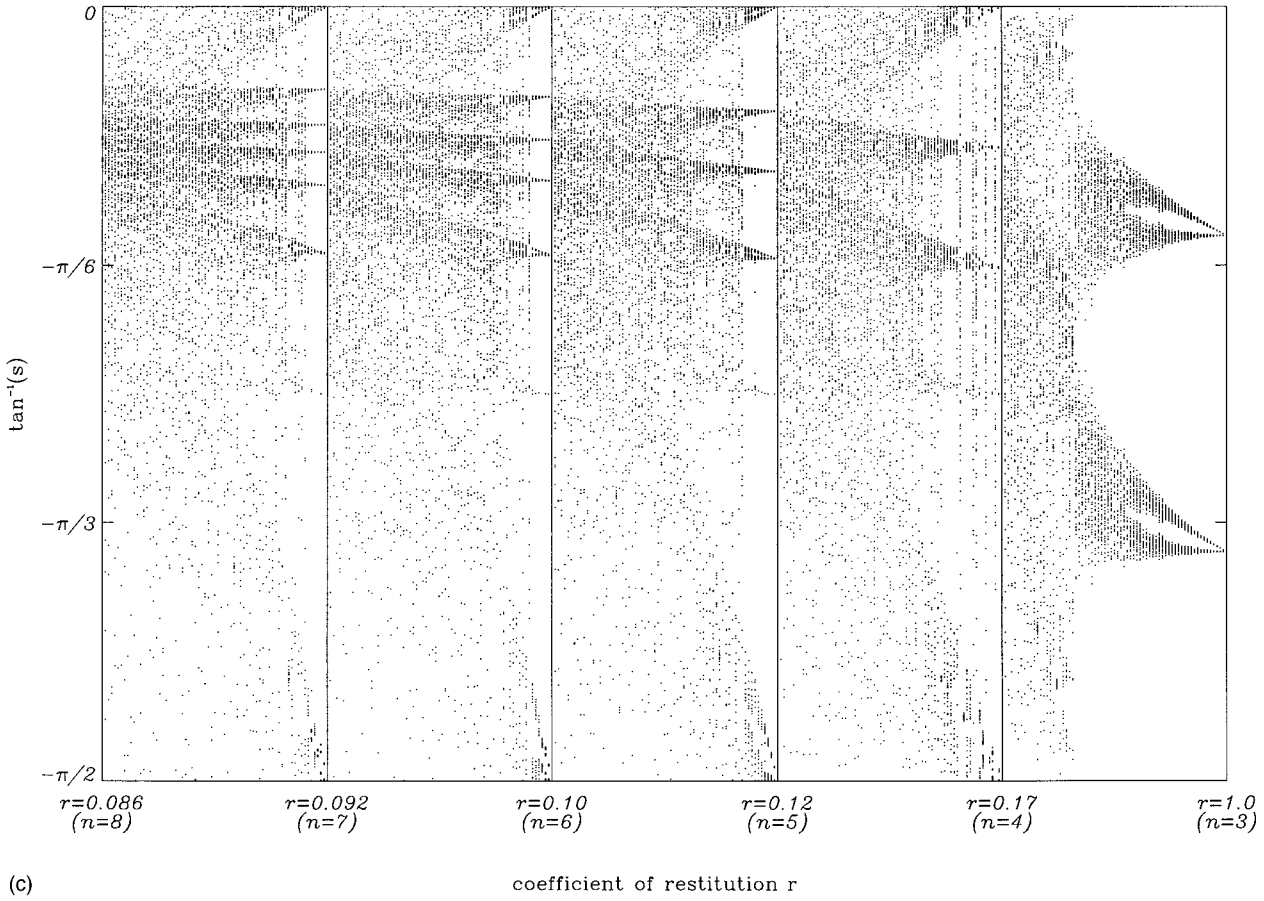


FIG. 5 (*Continued*).

### B. The elastic case ($r=1$)

In this section we analyze the recursions for the case $r=1$. It can be shown that the construction of Sec. I B reduces the dynamics of three perfectly elastic particles on a circle to a billiard with specular reflections. The results we derive could be shown perhaps more easily using conventional analysis of specular billiard systems. However our motivation is to extend some of the techniques used here to the case $r\neq 1$ where the reflections are no longer specular. It is therefore instructive to study the elastic case using recursions (1.9).

For $r=1$, $b=1/2(1+r)=1$, and recursions (1.9) become

$$\begin{pmatrix} s_{n+1} \\ d_{n+1} \end{pmatrix} = \begin{cases} \begin{pmatrix} -1/(1+s_n) \\ -d_n s_n \end{pmatrix} & \text{if } 0<z_n=\dfrac{-d_n s_n}{1+s_n} \\ \begin{pmatrix} 1/s_n \\ 1+d_n s_n \end{pmatrix} & \text{otherwise,} \end{cases} \tag{2.2}$$

with $d_0\in(0,1)$ and $s_0\in(-\infty,0)$ such that $-d_0 s_0\in(0,1)$. Let us denote the $s$ mappings by $f_1$ and $f_2$, respectively,

$$f_1(s)=-1/(1+s),$$

$$f_2(s)=1/s.$$

Now note that $s_n\in(-\infty,0)$ can be partitioned into two open intervals, $I\equiv(-1,0)$ and $I'\equiv(-\infty,-1)$. (For convenience, $s=-1$ has been excluded, as it generates a simple six-segmented periodic trajectory with $s_n=-1$ for all $n$ that is irrelevant for our purposes). We see that $f_1(I)=f_2(I)=I'$, $f_1(I')=(0,\infty)$, and $f_2(I')=I$. Thus, if we consider $s_n\in I$, there are only two possibilities for $s_{n+2}\in I$: $s_{n+2}=f_2\circ f_1(s_n)$ or $s_{n+2}=f_2\circ f_2(s_n)$; which mapping is selected depends on $z_n$. Denote these by $A$ and $B$, respectively. Then in the billiard, these ''two steps'' appear as in Fig. 6, and we can consider the dynamics as an evolution under $A$ and $B$

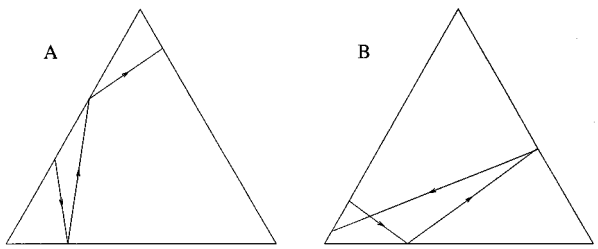


FIG. 6. The two types of maps that comprise the motion when $r=1$. Type $A$ is composed of $f_{\mathrm{I}}$ followed by $f_{\mathrm{II}}$, while type $B$ is two successive applications of $f_{\mathrm{II}}$.

$$\begin{pmatrix} s_{n+2} \\ d_{n+2} \end{pmatrix} = \begin{cases} \begin{pmatrix} -1-s_n \\ 1+\dfrac{d_n s_n}{1+s_n} \end{pmatrix} & \text{for } A, \text{ where } z_n \in [0,1] \\ \begin{pmatrix} s_n \\ 1+d_n+\dfrac{1}{s_n} \end{pmatrix} & \text{for } B, \text{ where } z_n \notin [0,1]. \end{cases} \tag{2.3}$$

Note that these equations imply that, given $s_0 \in I$, the only values that $s_n \in I$ can assume (where $n$ is even) are $s_0$ and $-(1+s_0)$.

As the quantity $z_n = -s_n d_n/(1+s_n)$ is what determines whether the next step is an $A$ or a $B$, we look at the evolution of $z_n$ under (2.3),

$$A: z_{n+2} = -\frac{1+s_n}{s_n}(1-z_n),$$

$$B: z_{n+2} = -(1-z_n).$$

The only dependence on $s_n$ is through a factor $\sigma_n \equiv -(1+s_n)/s_n$. These recursions can equivalently be written in terms of $(z_n, \sigma_n)$ using (2.3)

$$\begin{pmatrix} z_{n+2} \\ \sigma_{n+2} \end{pmatrix} = \begin{cases} \begin{pmatrix} \sigma_n(1-z_n) \\ 1/\sigma_n \end{pmatrix} & \text{for } A, \text{ where } z_n \in [0,1] \\ \begin{pmatrix} z_n - 1 \\ \sigma_n \end{pmatrix} & \text{for } B, \text{ where } z_n \notin [0,1]. \end{cases} \tag{2.4}$$

Hence $\sigma_n$ takes only two values, $\sigma_0$ or $1/\sigma_0$, which are both positive for $s_0 \in (-1,0)$. Without loss of generality, we assume that $\sigma_0 > 1$ (this is merely a statement that we label the first $s \in (-1/2,0)$ as the initial condition) and distinguish between $A^+$ and $A^-$, so that the recursions (2.4) are now comprised of three maps

$$A^+ (\text{when } z_n < 1 \text{ and } \sigma_n = \sigma_0 > 1):$$

$$\begin{pmatrix} z_{n+2} \\ \sigma_{n+2} \end{pmatrix} = \begin{pmatrix} \sigma_0(1-z_n) \\ 1/\sigma_0 \end{pmatrix},$$

$$A^- (\text{when } z_n < 1 \text{ and } \sigma_n = 1/\sigma_0 < 1):$$

$$\begin{pmatrix} z_{n+2} \\ \sigma_{n+2} \end{pmatrix} = \begin{pmatrix} (1/\sigma_0)(1-z_n) \\ \sigma_0 \end{pmatrix}, \tag{2.5}$$

$$B (\text{when } z_n > 1): \quad \begin{pmatrix} z_{n+2} \\ \sigma_{n+2} \end{pmatrix} = \begin{pmatrix} (z_n - 1) \\ \sigma_n \end{pmatrix}.$$

From (2.5) it is clear (i) that as long as $z < 1$, the system evolves under an alternating sequence of $A^+$ and $A^-$ steps; (ii) that since $z$ can become larger than one only through an $A^+$ step, $B$ steps can be preceded by an $A^+$ (but never an $A^-$); and (iii) that a series of $B$ steps, which acts to reduce $z$, will continue until $z$ is less than one, at which point the next step must be an $A^-$, since the $B$ sequence was initiated with an $A^+$ step and $\sigma$ does not change under $B$. From these three facts, we conclude that the sequence of maps must assume the form

$$\ldots B^{m_2}(A^+A^-)^{n_2}B^{m_1}(A^+A^-)^{n_1}\cdots . \tag{2.6}$$

The action of $A^+A^-$ can be calculated explicitly from (2.5); noting that $A^-$ is applied first, then $A^+$, giving

$$A^+A^-: \quad \begin{pmatrix} z_{n+4} \\ \sigma_{n+4} \end{pmatrix} = \begin{pmatrix} z_n + (\sigma_0 - 1) \\ 1/\sigma_0 \end{pmatrix}. \tag{2.7}$$

The dynamics generating the series (2.6) is essentially a translation of $z$ by $\sigma_0 - 1$ around the unit circle and thus is one dimensional. It is not difficult to show that $n_i$ and $m_i$ of (2.6) are limited by the value $\sigma_0$

$$1 \leq n_i \leq \left[\left[\frac{1}{\sigma_0 - 1}\right]\right] + 1 = n_{\max}$$

$$1 \leq m_i \leq [[\sigma_0]] = m_{\max}$$

where [[ ]] is the least integer function. Since the dynamics of $z$ is a circle map, the sequence of $z$ values [and hence (2.6)] is periodic whenever the translational shift $(\sigma_0 - 1)$ is rational, i.e., $s_0$ is rational. This can be intuitively understood by considering the particles on the ring. Since they collide elastically and are identical, the situation is equivalent to the particles passing through each other, and the quantity $s_0$ is then just the relative rotation rates of the three particles. When this is rational, there is periodic behavior. Conversely, in the generic case where $s_0$ is irrational, we do not see repeating orbits, but rather quasiperiodic behavior. To quantify this, let us say that at each moment of collision we take a snapshot of the system. In this picture, two particles are next to each other and the third particle is elsewhere on the ring. Let $\delta$ denote the smallest distance between the pair and the third particle as measured along the ring. Compiling a list of $\delta$ values from collision to collision, a probability distribution is obtained. For rational $s_0$, the orbit, and hence the $\delta$ values, are periodic, and the distribution is a collection of spikes. However, when $s_0$ is irrational, the distribution will be smooth and moreover uniform between $\delta = 0$ and $\delta = 1/2$. Regarding the billiard, this is equivalent to saying that the trajectories have equal probability of leaving a side at any point along its length. These points of emergence are dense along each side, and hence the resultant trajectory appears to fill the triangle. In terms of the mapping (1.9) in the $(s_n, d_n)$ plane, the distribution of $\delta$ is merely the distribution of $\min(d_n, 1-d_n)$.

### C. The nearly elastic regime ($r = 1 - \epsilon$)

The general examination of the quasielastic regime in Sec. II A showed that the dynamics of the billiard when $r$ is near but not equal to one is pseudoperiodic and strikingly distinct from that when the particles are elastic. Figure 7 shows both the uniform distribution expected for the elastic case as well as the distribution of $\delta$ obtained numerically for $\epsilon \neq 0$. Not only is the evenness of the $r = 1$ case lost, but there seems to be a region of $\delta$ values that is forbidden entirely. The corresponding trajectory in the triangle is confined to a stripelike region (see Fig. 8) in which the impacts on the sides are either very close to a corner (so $\delta$ is nearly zero), or practically in the middle of the opposite side (so $\delta$ is nearly one half). Numerically, the formation of this stripe is robust,

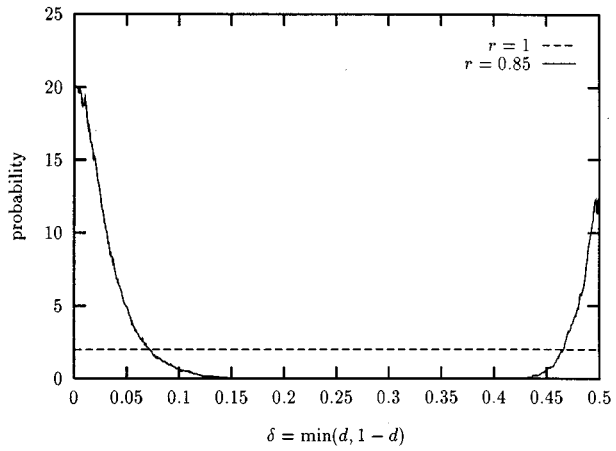


FIG. 7. The probability distributions for $\delta=\min(d_n,1-d_n)$ for $r=1$ and $r=1-\epsilon=0.85$. Notice the clear distinction in the shape of the curves. This difference is maintained for all *nonzero* $\epsilon$ less than approximately 0.27. The peaks become more diffuse (i.e., the region of forbidden $\delta$'s shrinks) as $\epsilon$ gets larger. For $\epsilon=1-r=0.15$, we have $\delta\lesssim 0.14$ or $\delta\gtrsim 0.43$.

i.e., for all random initial conditions that we have tried, after some transients, the trajectory will settle into this sort of path and stay there. Thus this stripe seems to correspond to some attractive, stable region of phase space.

A close inspection of the simulations shows that the stripe in the billiard is produced by some very simple dynamics of the three particles on the ring. If we are in a reference frame such that the particles' total momentum is zero, the stripe corresponds to one particle remaining relatively still as the others bounce back and forth almost symmetrically on either side of it. When the two outer particles are near the center one, they are not hitting it simultaneously; rather the center one rattles quickly back and forth—it bounces against one, then the other, then the first one again—before the outer particles move away to the other side of the ring where they bounce off each other and return to the center particle to repeat the process (see Fig. 9). In the billiard, the stripe trajectory can be decomposed into two simple building blocks—call them $T$ for tooth and $F$ for flip—as shown in Fig. 10. The tooth corresponds to the series of collisions shown in Fig. 9, while the flip is the trajectory that appears when the collision order during rattling changes.

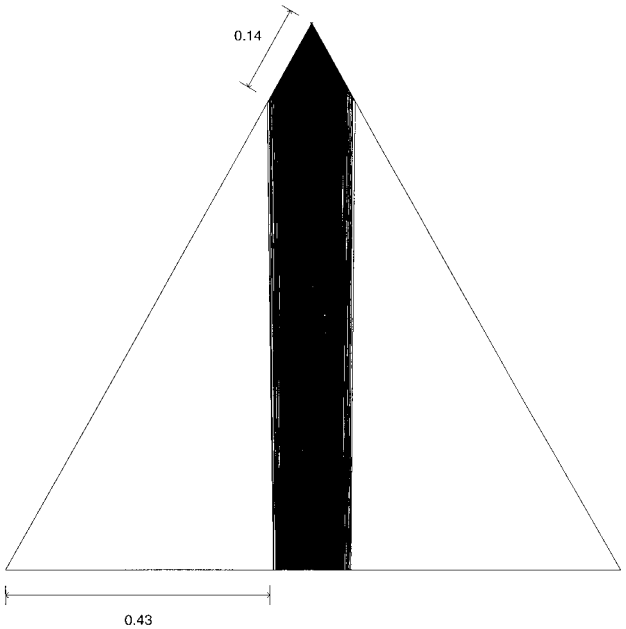


FIG. 8. Ten thousand bounces in the trajectory of a billiard at $r=0.85$. We have used random initial conditions, but removed the first 200 bounces, as they are transients. Once the system begins the stripe behavior, it continues indefinitely. The limits on $\delta$, as seen in Fig. 7, have been marked on this plot.

Comparing Fig. 4 and Fig. 10 demonstrates that the tooth and flip are written

$$T\begin{pmatrix} s_n \\ d_n \end{pmatrix} = f_{\mathrm{II}}\circ f_{\mathrm{I}}\circ f_{\mathrm{II}}\circ f_{\mathrm{I}}\begin{pmatrix} s_n \\ d_n \end{pmatrix} \tag{2.8a}$$

$$F\begin{pmatrix} s_n \\ d_n \end{pmatrix} = f_{\mathrm{II}}\circ f_{\mathrm{I}}\circ f_{\mathrm{II}}\circ f_{\mathrm{II}}\begin{pmatrix} s_n \\ d_n \end{pmatrix}. \tag{2.8b}$$

Thus our numerical findings suggest that a trajectory in the stripe region can be represented symbolically by a series of $T$'s and $F$'s

$$\ldots T^{\overline{n_{\nu+3}}}FT^{n_{\nu+2}}FT^{n_{\nu+1}}FT^{n_\nu}F\cdots \tag{2.9}$$

and simulations show that the integers $n_\nu$ range from 0 to some maximum value $n_{\max}$ which depends on $\epsilon=1-r$.

Since numerical evidence indicates the robustness of the stripe, we can observe $(s,d)$ not after each collision, but after each $T^n\circ F$ step. While this approach cannot describe fully all possible trajectories within the triangle, it turns out that it does provide a complete description of the behavior once a trajectory has settled into a stripe. We have not proven that the stripe is globally attracting, but we can nonetheless show that the mapping $T^n\circ F$ has an invariant region in the $(s,d)$ plane, and thus the stripe is a stable, self-contained region of phase space. Numerics show that this stripe region exists for $\epsilon\lesssim 0.27$.

Trajectories can now be represented as a sequence of points in the $(s^\nu,d^\nu)$ plane where $(s^{\nu+1},d^{\nu+1})=T^{n_\nu}\circ F(s^\nu,d^\nu)$ and $n_\nu$ is itself a function of $s^\nu$ and $d^\nu$. For convenience, instead of working in terms of $(s^\nu,d^\nu)$, define $d_1^\nu=-s^\nu d^\nu$; in the $(s^\nu,d_1^\nu)$ plane, the simulations demonstrate that the region of interest is near $(-1/2,1/2)$. A typical trajectory is shown in Fig. 11(a). Notice that for a given $s^\nu$, there is both an upper and lower bound on the values $d_1^\nu$ can assume. The former is due to the fact that $d^\nu<1$, so $d_1^\nu=-s^\nu d^\nu<-s^\nu$. The latter bound exists because these $(s,d_1)$ are plotted when the next step is a flip. From (2.8b) we see that the first map in a flip is $f_{\mathrm{II}}$, i.e., the $z$ associated with $(s^\nu,d^\nu)$ must be greater than one or less than zero. The latter is not possible in this region, but the former implies that $1<z^\nu=-rs^\nu d^\nu/(s^\nu+b)=rd_1^\nu/(s^\nu+b)$, so $d_1^\nu>(s^\nu+b)/r$.

The next step is to look at the dependence of $n_\nu$ on $(s^\nu,d_1^\nu)$. Given an $(s^\nu,d_1^\nu)$, we can compute the corresponding $n_\nu$ by applying $F$ followed by a series of $T$'s until $z$ is greater than one or less than zero. If each $(s^\nu,d_1^\nu)$ is labeled by the appropriate $n_\nu$, the continuity of the $T$ and $F$ maps ensures that the plane is divided into distinct cells, each cor-

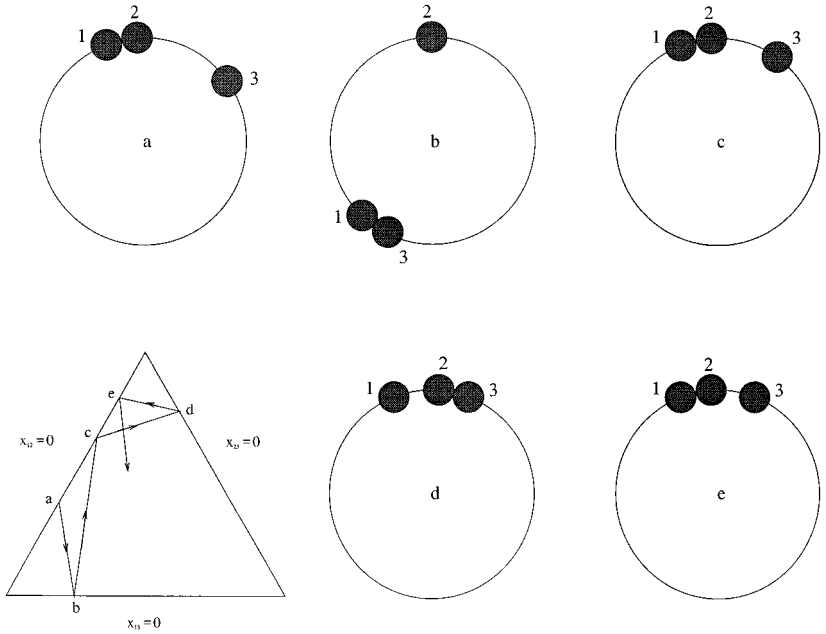


FIG. 9. The motion in configuration space that corresponds to the stripe in the billiard picture. The series of collisions that give rise to the tooth ($T$) trajectory are shown explicitly. Step $e$ is not really part of this tooth, but rather the first segment of the next one (the equivalent of $a$). A flip would be similar, but the last three collisions would be 23, 12, 23 (rather than 12, 23, 12).

responding to a different $n_\nu$ [see Fig. 11(b)]. Notice that a typical trajectory does not visit all such $n_\nu$ cells. How (and why) the trajectory is limited to $n_\nu = 0,1,\ldots,n_{\max}$ will be discussed later in this section. However, simulations allow us to compute $n_{\max}$ at various $\epsilon$ (see Fig. 12); the data show that $n_{\max}$ scales as $\epsilon^{-1/2}$ as $\epsilon \to 0$.

Numerical observation of the stripe has lead us to consider $T^{n}\circ F$ as the basic recursion. For small $\epsilon$, the region of interest in the $(s^\nu, d_1^\nu)$ plane is near $(-1/2,1/2)$ and has a width in the $s^\nu$ direction that scales roughly as $\epsilon^2$. Returning to the analytic expressions for $T$ and $F$ (2.8), we can look at $T^{n}\circ F$ in the limit $\epsilon \to 0$. Linearizing this recursion within each $n_\nu$ cell gives

$$s^{\nu+1} \approx s^* - \alpha^{n_\nu+1}(s^\nu + 1 + s^*) \tag{2.10}$$

$$\begin{aligned} d_1^{\nu+1} \approx & -d_1^\nu \beta^{n_\nu+1} + \beta^{n_\nu}\left[\alpha - \gamma + s^*\left(\alpha - 2 - \frac{\beta}{1-\epsilon}\right)\right] \\ & + \gamma\,\frac{1-\beta^{n_\nu}}{1-\beta} + \alpha(1+s^*)\left(\alpha + \frac{\beta}{1-\epsilon}\right)\frac{\alpha^{n_\nu}-\beta^{n_\nu}}{\alpha-\beta} \\ & + s^\nu\left(\alpha + \frac{\beta}{1-\epsilon}\right)\frac{\alpha^{n_\nu+1}-\beta^{n_\nu+1}}{\alpha-\beta}, \end{aligned}$$

where, as noted above, $n_\nu$ is itself a function of $s^\nu$ and $d_1^\nu$. The parameters in the above equations are all just functions of $\epsilon$

$$\phi = \sinh^{-1}\left[\frac{\epsilon(2-\epsilon)}{8(1-\epsilon)}\right], \tag{2.11}$$

$$s^* = (1-\epsilon/2)/[\sinh(\phi) - \cosh(\phi) - 1],$$

$$\alpha = e^{4\phi},$$

$$\beta = (1-\epsilon)^2/[1 - 2\sinh(\phi) + 2\sinh^2(\phi)],$$

$$\gamma = -s^*\left(1 + \frac{\beta}{1-\epsilon}\right) - \beta(1-\epsilon/2)/(1-\epsilon).$$

From (2.10), the linearization is of the form

$$\begin{pmatrix} s^{\nu+1} \\ d_1^{\nu+1} \end{pmatrix} = \begin{pmatrix} \kappa(n_\nu) \\ \mu(n_\nu) \end{pmatrix} + \begin{pmatrix} -\alpha^{n_\nu+1} & 0 \\ \rho(n_\nu) & -\beta^{n_\nu+1} \end{pmatrix}\begin{pmatrix} s^\nu \\ d_1^\nu \end{pmatrix}, \tag{2.12}$$

where the expressions for $\kappa(n_\nu)$, $\mu(n_\nu)$, and $\rho(n_\nu)$ can be readily determined from (2.10) and (2.11). By comparison with the exact analytic expression (2.8), it can be shown that the error introduced by the linearization (2.10) is of order $\epsilon^4$ or smaller. The linearized mapping is itself rather involved, due to the complex dependence of the coefficients on $\epsilon$. However some conclusions can still be drawn merely from the form of the mapping (2.12).

For instance, we expect to find a fixed point in each $n_\nu$ cell. Indeed, solving the recursion

$$\begin{pmatrix} s \\ d_1 \end{pmatrix} = T^{n_\nu}\circ F\begin{pmatrix} s \\ d_1 \end{pmatrix}$$

either analytically using the linearized map (2.10) or computationally (using the full recursions and Newton's method), we discover that there is one such fixed point per each $n_\nu$ cell for $n_\nu$ between zero and a maximum value $n_{\max}^{\text{fix}}$ that depends on $\epsilon$ [see Fig. 11(b)]. It is important to note that $n_{\max}^{\text{fix}} > n_{\max}$, where $n_{\max}$ is the biggest $n_\nu$ observed in a stable trajectory [see after Eq. (2.9)]. In fact, the analytic formula enable us to calculate $n_{\max}^{\text{fix}}$ for small $\epsilon$ and observe how it scales as $\epsilon \to 0$

$$n_{\max}^{\text{fix}} = -1 + 2\sqrt{1 + 3/\epsilon} \approx 2\sqrt{3}\,\epsilon^{-1/2}. \tag{2.13}$$

This provides an upper bound on $n_{\max}$.

The linearized expression also provides information about the stability of the fixed points in the limit of small $\epsilon$. Equa-

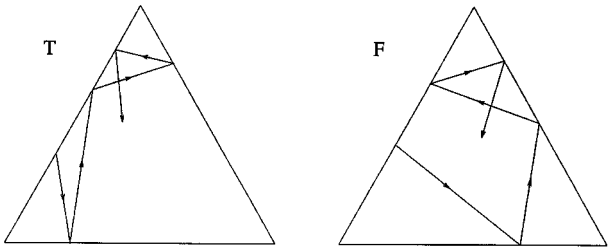


FIG. 10. The two types of motion that comprise the stripe. The tooth ($T$) only uses two of the corners, while the flip ($F$) visits all three.

tion (2.12) shows that each fixed point has a stable and unstable direction, (0,1) and $[\beta-\alpha,\ \alpha+(\beta/1-\epsilon)]$, respectively, with corresponding eigenvalues $-\beta^{n_\nu+1}$ and $-\alpha^{n_\nu+1}$, where $\alpha$ and $\beta$ are as defined in Eq. (2.11). For $\epsilon>0$, $\alpha>1>\beta>0$. The existence of these competing stable and unstable directions within each $n_\nu$ cell draws the trajectory toward the unstable directions into a linelike formation. Thus we do not expect a full exploration of the phase space plane. Calculating numerically the fractal dimension of the set of points comprising the trajectory in the $(s^\nu,d_1^\nu)$ plane under repeated application of $T^{n_\nu}\circ F$ [Fig. 11(a)], we find that the dimension is roughly 5/3, rather than two.

The presence of the fixed points and their location explain why the actual number of distinct $n_\nu$ cells visited by a trajectory ($n_{\max}$) is less than the number of fixed points ($n_{\max}^{\text{fix}}$). Because the eigenvalues, $-\beta^{n_\nu+1}$ and $-\alpha^{n_\nu+1}$, are negative, a given $n_\nu$ cell is stretched, contracted, and rotated under the map $T^{n_\nu}\circ F$ [see Fig. 11(c) for some examples]. Thus a point in that cell can be mapped into several neighboring regions, as well as back into the original cell. What determines whether a region is visited regularly by a typical trajectory is not so much where it is mapped to, but where it is mapped from. For example, in Fig. 11(c), $n_\nu=8$ is mapped into the cells $n_\nu=5$, 6, 7, and 8, and hence $n_\nu=9$ has no sources from a lower $n_\nu$ cell. Meanwhile, $n_\nu=7$ is mapped into $n_\nu=4$, 5, 6, 7, and 8, thus $n_\nu=8$, is in fact fed into from a lower $n_\nu$ cell. Thus any trajectory starting in $n_\nu=9$ or higher can only decrease (or, at best, hold constant) its $n_\nu$ value, while for lower $n_\nu$, the values can move up or down. Hence stable trajectories will be trapped in the region below $n_\nu=9$. Thus, in this example ($\epsilon=0.1$), $n_{\max}$ is eight. In general: $n_{\max}$ is the greatest $n_\nu$ such that a section of the $(n_\nu-1)$ cell is mapped into the $n_\nu$ cell. Using the analytic forms, we can quantify this condition, and thus write an expression that describes the scaling of $n_{\max}$ as $\epsilon\to 0$:

$$n_{\max}\approx 2.4\epsilon^{-1/2}, \tag{2.14}$$

which is consistent with the data obtained by examining actual trajectories at various $\epsilon$ (see Fig. 12).

In summary, the asymptotic behavior of the dynamics of three particles moving on a ring changes sharply when their collisions become slightly inelastic. While for the case of totally elastic particles, the phase space that is explored consists of four $s$ values and all $d\in(0,1)$ (a strictly one-dimensional space), numerical simulations indicate that in the presence of inelasticity ($0<\epsilon\lesssim 0.27$) the system is

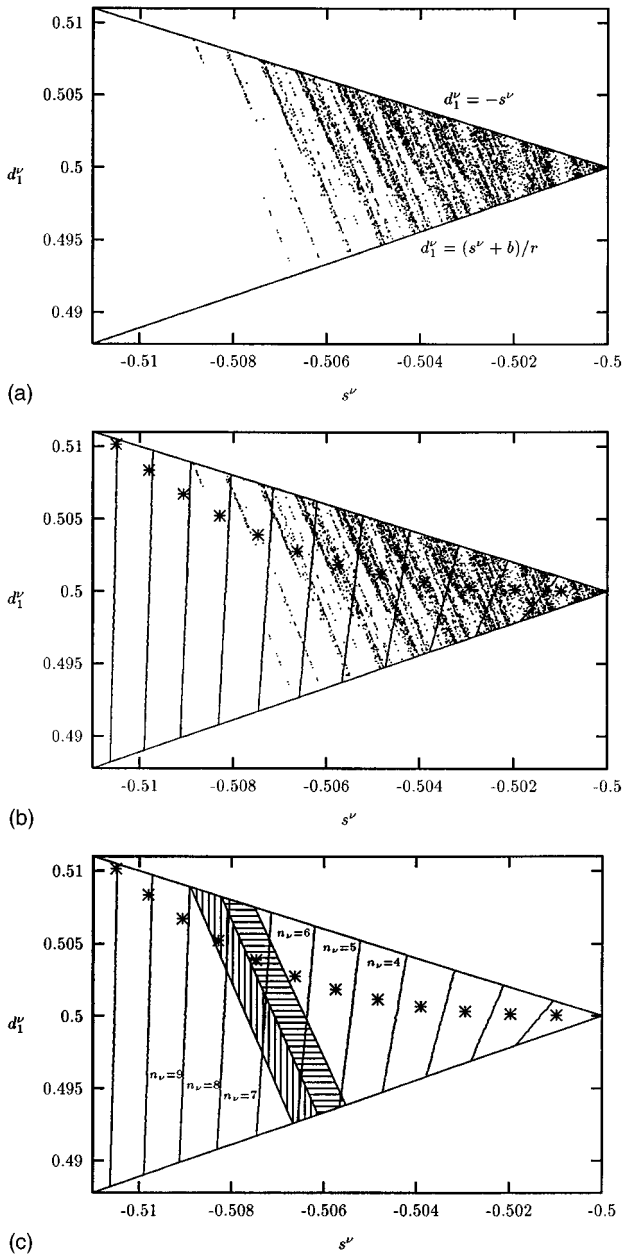


FIG. 11. A trajectory in the $(s^\nu,d_1^\nu)$ plane for $\epsilon=0.1(r=1-\epsilon=0.9)$. (a) This is a sample of the long-term behavior of a trajectory with random initial conditions (5000 points). (b) The same trajectory as in (a), but here the $n_\nu$ regions are outlined and the fixed points marked by stars. Notice that the number of regions visited by the trajectory ($n_{\max}$) is less than the number of regions for which there exist fixed points ($n_{\max}^{\text{fix}}$). (c) The action of the map $T^{n_\nu}\circ F$ on two $n_\nu$ regions: $n_\nu=7$ (horizontal shading) and $n_\nu=8$ (vertical shading).

trapped into a fractal region of phase space and generates a stripe in the triangle. Therefore the behavior in the $\epsilon\neq 0$ regime does not approach that for the elastic case, and the limit $r\to 1$ is singular. There is no analytic evidence to show that this stripe corresponds to a globally attractive region of phase space, although simulations suggest that its formation is robust. On the other hand, by studying the map associated with the stripe ($T^n\circ F$) and its linearized version (2.10) in the $(s^\nu,d_1^\nu)$ plane we have been able to understand the dynamics

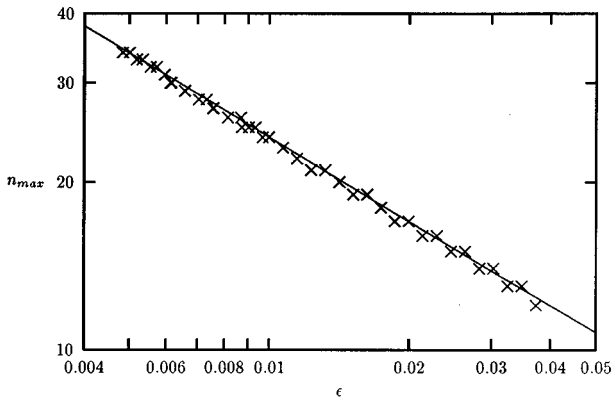


FIG. 12. A comparison of simulational and analytic values for $n_{\max}$ as a function of $\epsilon$. The crosses are values obtained by examining typical trajectories over $10^6$ applications of $T^{n_0}F$. The solid line is the analytic expression (2.14): $n_{\max}\approx 2.4\epsilon^{-1/2}$.

of the trajectories once they have settled into the stripe region and to show that they will remain there.

### III. THE STRONGLY INELASTIC REGIME: $r\leqslant r_{cr}$

In Sec. I it was pointed out that motion restricted to any corner of the billiard is governed by the dynamics on the infinite line. Thus for $r\leqslant r_{cr}$ the corners of the triangle can become attracting. A ray incident onto a corner will either zigzag into the origin (collapse) or eventually leave (escape). If the latter occurs, the trajectory is then incident onto one of the other two corners and the same options are present. For motion on the ring, the question therefore arises whether all initial conditions will eventually result in collapse.

In this section it will be shown that the answer depends entirely on the initial slopes. For $r\leqslant r_{cr}$, there is a set of slopes that generate trajectories that will never collapse, but continue to change corners indefinitely. This set turns out to be fractal and its dimension at $r=r_{cr}$ will be estimated.

The motion within a corner is described by $f_I$ of (1.9)

$$\begin{pmatrix} s_{n+1} \\ d_{n+1} \end{pmatrix} = f_I \begin{pmatrix} s_n \\ d_n \end{pmatrix} = \begin{pmatrix} -r/(b+s_n) \\ -s_n d_n \end{pmatrix}. \tag{3.1}$$

For $r\leqslant r_{cr}=7-4\sqrt{3}$, the map $f_1: s_n \to s_{n+1}$ has two real fixed points given by

$$s_{\pm}^{*}=\frac{b}{2}\,(-1\pm\sqrt{1-4\eta}), \tag{3.2}$$

where $b=(1+r)/2$ and $\eta=r/b^2$. Note that $-1<s_-^*<s_+^*<0$. Here $s_-^*$ is unstable and $s_+^*$ is stable, with a basin of attraction $(s_-^*,0)$.

The motion on the circle will in general be a sequence of mapping $f_I$ and $f_{II}$ of (1.9) depending on the value of $z_n=-rs_n d_n/(b+s_n)$ (1.8). Consider a segment of the trajectory described by $(s_0,d_0)$ and assume that $z_0\in(0,1)$ so that the next map is $f_I$. If $s_0>s_-^*$, the slope will move monotonically towards $s_+^*$ under repeated applications of $f_I$ and hence $s_n\in(-1,0)$ for all $n$. Meanwhile, from (3.1) it is seen that

$$d_n=d_0\prod_{j=0}^{n-1}(-s_j)$$

indicating that in this case both the separations $d_n$ and $z_n=-d_{n+1}s_{n+1}$ will decrease monotonically to zero. In particular, this implies that $z_n\in(0,1)$ for all $n$ and indeed all subsequent mappings must be $f_I$, i.e., there is no corner change and the trajectory zigzags into the original corner. One therefore arrives at the following:

*Proposition 1*. Let $r\leqslant r_{cr}$. If the evolution (1.9) generates a segment $(s_n,d_n)$ whose slope satisfies $s_n\geqslant s_-^*$, then the subsequent trajectory collapses in the corner associated with that segment.

On the other hand, if $s_n<s_-^*$, the trajectory evolves via $f_I$ until $z\notin(0,1)$ and there is a corner change via map $f_{II}$ of (1.9). Let $s_0^k$ denote the slope right after the $k$th corner change, let $C$ denote the evolution of the slope within a given corner,

$$C: s_{n+1}^k=f_1(s_n^k)=-r/(b+s_n^k) \tag{3.3}$$

and, assuming that the trajectory undergoes $n_k$ bounces in the $k$th corner, denote by $D$ the corner changing step,

$$D: s_0^{k+1}=f_2(s_{n_k}^k)=-r/(b-1-s_{n_k}^k). \tag{3.4}$$

The evolution of the billiard is then described by the sequence

$$\ldots DC^{n_{k+2}}DC^{n_{k+1}}DC^{n_k}\ldots$$

It can be readily shown from (3.3) that, for $-\infty<s_0^k<s_-^*$, $s_n^k$ is monotonically decreasing with $n$, i.e., with repeated applications of $C$. This continues until a $D$ step occurs, the condition for which is either

$$\text{(i)}\, z_n^k<0\Leftrightarrow s_n^k<-b,$$

$$\text{(ii)}\, z_n^k>1\Rightarrow -b<s_n^k<-1/2,$$

where $-b<s_n^k<-1/2$ is a necessary, but not sufficient, condition for $z_n^k>1$.

Consider (i) first. The step $D$ maps the interval $I=(-\infty,-b]$ into $[-1,0)$. Recall that the domain of attraction of the fixed points is $[s_-^*,0)\subset[-1,0)$. Owing to the monotonicity of $D$ in $I$, there exists an $\overline{s}\in I$ such that $f_2(\overline{s})=s_-^*$ and thus $\overline{s}$ partitions $I$ into the disjoint intervals $I_c^0=(-\infty,\overline{s}]$ and $I_f^0=(\overline{s},-b]$ which are mapped under $D$ into $[s_-^*,0)$ and $[-1,s_-^*)$, respectively. From (3.4) we find that

$$\overline{s}=\frac{b}{2}\left(1-\frac{2}{b}+\sqrt{1-4\eta}\right)$$

and thus, for $r\leqslant r_{cr}$, $\overline{s}$ is, in fact, between $-1$ and $-b$. One therefore obtains

*Proposition 2*. If $s_n^k\in(-\infty,-b]$, the next step is $D$, i.e., a corner change. Furthermore, if $s_n^k\in I_c^0=(-\infty,\overline{s}]$, then $s_0^{k+1}\in[s_-^*,0)$ and by Proposition 1 the trajectory collapses in the new $[(k+1)^{th}]$ corner. Conversely, a sufficient condition for the trajectory not to collapse in this new corner is $s_n^k\in I_f^0=(\overline{s},-b]$.

Consider now (ii), the second possibility for a corner change. Here, if $s_n^k \in (-b,-1/2)$, one must look at the $d_n^k$ value to determine if $z_n^k$ is actually greater than one. If it is, the resulting $D$ step will map $(-b,-1/2)$ into $(-2,-1)$, a subset of $I_c^0$. Thus by Proposition 2, the trajectory immediately undergoes another $D$ step and is moved to a new corner in which it must collapse. If, on the other hand, $s_n^k \in (-b,-1/2)$ but $d_n^k$ is such that $z_n^k$ is not greater than one, the next step must be $C$. A short calculation shows that $C$ maps $(-b,-1/2)$ into $(-\infty,-2)$, also a subset of $I_c^0$. Therefore, by Proposition 2, the next step after $C$ must be a $D$ and the trajectory will collapse in the corner $D$ takes it to. These two results are summarized as

*Proposition 3*. If $s_n^k \in (-b,-1/2)$, then the subsequent trajectory will collapse after at most two more corner changes.

Note that Proposition 3 is, again, independent of $d_n^k$.

Now consider the preimages of $I_c^0$ and $I_f^0$ under $C$

$$I_c^n \equiv C^{-n}(I_c^0) = \{s | f_1^n(s) \in I_c^0\}, \tag{3.5a}$$

$$I_f^n \equiv C^{-n}(I_f^0) = \{s | f_1^n(s) \in I_f^0\}. \tag{3.5b}$$

Since $f_1$ is monotonic in $(-b,0)$, the sets $I_c^n$ and $I_f^n$ are mutually disjoint (i.e., $I_c^n \cap I_f^m = \emptyset$ for all $m$, $n$ and $I_c^n \cap I_c^m = I_f^n \cap I_f^m = \emptyset$ for all $m \neq n$). Letting

$$I_c = \bigcup_{n=0}^{\infty} I_c^n \quad \text{and} \quad I_f = \bigcup_{n=0}^{\infty} I_f^n, \tag{3.6}$$

it readily follows that:

$$I_c \cup I_f = (-\infty, s_-^*). \tag{3.7}$$

In the discussion leading to Proposition 3 it has also been shown that $(-b,-1/2) \subset I_c^1$ and therefore Propositions 1–3 can be summarized as

*Proposition 4* Consider a trajectory defined by its segments $(s_n, d_n)$. (a) If $s_n \in [s_-^*, 0)$ for some $n$, the trajectory collapses in the corner associated with that segment. (b) If $s_n \in I_c$, the subsequent trajectory collapses after at most two more corner changes. (c) The trajectory will never collapse in any corner if and only if $s_n \in I_f$ for all $n$. Moreover, the symbolic sequences for trajectories of the types (a) and (b) are of the form

$$C^{\infty} D C^{n_k} D C^{n_{k-1}} \cdots$$

whereas for (c) the sequences are of the form

$$\ldots C^{n_{k+1}} D C^{n_k} D C^{n_{k-1}} D \cdots$$

all the $n_k$'s being finite.

Proposition 4(c) establishes the necessary and sufficient condition for the noncollapsing trajectories and shows how the set of initial slopes giving rise to these is to be constructed. Assume an initial segment $(s_0^0, d_0^0)$ such that $s_0^0 \in I_f$. From (3.5b) and (3.6), $s_0^0 \in I_f^{n_0}$ for some unique $n_0$, indicating that it will take $n_0$ $C$ steps to map $s_0^0$ into $s_{n_0}^0 \in I_f^0$. Without loss of generality, assume therefore $s_0^0 \in I_f^0$ and denote by $C^n$ the projection $I_f \to I_f^0$. By Proposition 2, the next step is $D$. Since $D$ maps $I_f^0$ into $I_f \cup I_c$, by (3.6, 3.7) $s_0^1$ will lie in either $I_f^{n_1}$ or $I_c^{n_1}$ for some $n_1$. If the trajectory is to be noncollapsing, it is necessary that $s_0^1 \in I_f$.

Denote by $\Sigma_1^0$ the subset of initial slopes $s_0^0$ in $I_f^0$ that remain uncollapsed after the first corner change. Then $\Sigma_1^0 = I_f^0 \cap (C^n \circ D)^{-1}(I_f^0)$. Consider therefore the following recursion:

$$\Sigma_{j+1}^0 = \Sigma_j^0 \cap (C^n \circ D)^{-1}(\Sigma_j^0), \tag{3.8}$$

with $\Sigma_0^0 = I_f^0$. Note that $\Sigma_j^0$ is a monotonically decreasing sequence of sets, (i.e., $\Sigma_0^0 \supset \Sigma_1^0 \supset \Sigma_2^0 \ldots$), and hence define

$$\Sigma^0 = \lim_{j\to\infty} \Sigma_j^0 = \lim_{j\to\infty} \bigcap_{i=0}^{j} \Sigma_i^0. \tag{3.9}$$

Next extend the set $\Sigma^0 \subset I_f^0$ to its $C$ preimages: $\Sigma^n = C^{-n}(\Sigma^0)$ yielding

$$\Sigma = \bigcup_{n=0}^{\infty} \Sigma^n \subset I_f. \tag{3.10}$$

By construction, $\Sigma$ is the set of all points $s_0$ such that if $s_0 \in \Sigma$, then $s_n \in \Sigma$ for all $n$. What remains to be shown is that this set is nonempty. This can be done by explicit construction of $C^n \circ D$.

The solution of the slope recursion $C: s_{n+1} = f_1(s_n)$ for $r \leqslant r_{\rm cr}$ and $s_0 \in I_c \cup I_f$ is given by

$$s_n = -\frac{2r}{b}\left(1 - \frac{\coth[t(x_0+1-n)]}{\coth(t)}\right)^{-1} \tag{3.11}$$

where $t \equiv \cosh^{-1}(1/2\sqrt{\eta})$ and $b$ and $\eta$ are as defined after Eq. (3.2). The initial point is parameterized by $x_0 \in (0,\infty)$ and hence

$$s_0 = -\frac{2r}{b}\left(1 - \frac{\coth[t(x_0+1)]}{\coth(t)}\right)^{-1} \equiv s(x_0). \tag{3.12}$$

The function $s(x)$ is one to one, and thus one can equivalently consider the dynamics of $x$ which then becomes a translation, i.e.,

$$C: x_{n+1} = x_n - 1. \tag{3.13}$$

In order to characterize the sets $I_c^n$ and $I_f^n$ of (3.5), the following are needed:

$$s^{-1}(-b) = 1,$$

$$s^{-1}(-\infty) = 0,$$

$$s^{-1}(\overline{s}) = \overline{x} < 1,$$

$$\coth(t\overline{x}) = -1 + \frac{1-(r/b)}{\sqrt{(1/4)-\eta}}$$

and one finds that, in the $x$ representation,

$$I_f^n = \{x | n + \overline{x} < x \leqslant n+1\},$$

$$I_c^n = \{x | n < x \leqslant n + \overline{x}\}.$$

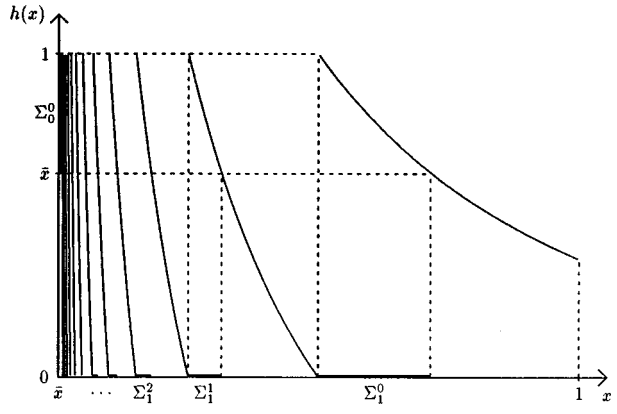


FIG. 13. The function $h(x)$ for $r=0.07<r_{\rm cr}$. The monotonic branches of $h(x)$ (only the first few are show for clarity) become steeper and more densely packed as $x\to\overline{x}$. Shown in bold are the subintervals $\Sigma_1^i$ of points that will be mapped into $\Sigma_0^0$ under the action of $h(x)$.

Denote by $g(x)$ the function corresponding to the mapping $D$ in the $x$ parametrization. Then $g:(\overline{x},1]\to(0,\infty)$ can be decomposed into its integer part $n(x)$ and the remainder $\Delta(x)$ such that

$$g(x)=n(x)+\Delta(x), \tag{3.14}$$

where $n$ is a positive integer and $0<\Delta(x)\leqslant 1$. Denote by $h(x)$ the function that corresponds to $C^n\circ D$ in the $x$ parametrization, so $h:(\overline{x},1]\to(0,1]$ and from (3.13) and (3.14) it is seen that

$$h(x)=\Delta(x). \tag{3.15}$$

The function $g(x)$ and hence $h(x)$ is straightforwardly worked out, yielding

$$\coth\{t[g(x)+1]\}=1+\coth(t\overline{x})-\coth(tx). \tag{3.16}$$

Note that this function is defined on $(\overline{x},1]$ only. It is readily verified that $\lim_{x\to\overline{x}}g(x)=\infty$ and $g(x)$ is monotonically decreasing on $(\overline{x},1)$. For $r=r_{\rm cr}$, $g(x)$ takes a particularly simple form:

$$g_{\rm cr}(x)=\overline{x}-1+\frac{\overline{x}^2}{x-\overline{x}}$$

with $\overline{x}=1/\sqrt{3}$. Figure 13 shows a plot of $h(x)$ for a typical value of $r<r_{\rm cr}$.

It follows immediately that

$$\Sigma_j\equiv\Sigma_j^0=\Sigma_0\cap h^{-j}(\Sigma_0), \tag{3.17}$$

where from now on the superscripts on $\Sigma$ will be omitted for the sake of clarity. Figure 13, which displays the general features of the function $h(x)$ for $r<r_{\rm cr}$, shows that $h^{-1}(\Sigma_0)$ is a countable union of disjoint intervals to be denoted by $\Sigma_1^i$ with the labeling $i=0,1,2,\ldots$ such that $\Sigma_1^0$ is the interval closest to $x=1$, $\Sigma_1^1$ is the next closest interval, etc. These intervals are

$$\Sigma_1^i=h_i^{-1}(\Sigma_0),$$

where $h_i$ are the monotonic branches of $h(x)$,

$$h_i(x)=g(x)-i,$$

with $i=0,1,2,\ldots$. Thus $\Sigma_2$ of Eq. (3.17) is a finer partitioning of each of the intervals of $\Sigma_1^i$ into the disjoint intervals $\Sigma_2^{i_1i_2}$ given by

$$\Sigma_2^{i_1i_2}=h_{i_2}^{-1}\circ h_{i_1}^{-1}(\Sigma_0),$$

so that

$$\Sigma_2=\bigcup_{i_1,i_2=0}^{\infty}\Sigma_2^{i_1,i_2}.$$

At level $n$, we therefore have the partition

$$\Sigma_n=\bigcup_{i_1,i_2,\ldots,i_n=0}^{\infty}\Sigma_n^{i_1i_2\ldots i_n} \tag{3.18a}$$

with

$$\Sigma_n^{i_1i_2\ldots i_n}=h_{i_n}^{-1}\circ\cdots\circ h_{i_2}^{-1}\circ h_{i_1}^{-1}(\Sigma_0) \tag{3.18b}$$

and as $n\to\infty$, the partitioning becomes more and more refined, resulting in the fractal set $\Sigma$. $\Sigma$ is nonempty and each of its elements is uniquely defined by the infinite sequence of integers $\{i_1,i_2,\ldots\}$ where $i_j=0,1,2,\ldots$. Thus $\Sigma$ is uncountable, and the dynamics on it is given by a shift: $C^n\circ D:\{i_1,i_2,\ldots\}\to\{i_2,i_3,\ldots\}$.

The Hausdorff dimension of $\Sigma$ can be estimated following Falconer [8], noting that the generators $h_i^{-1}$ are contractions and bi-Lifshitz, i.e., satisfy

$$p_i|x-y|\leqslant|h_i^{-1}(x)-h_i^{-1}(y)|\leqslant q_i|x-y| \quad \text{for all } x,y\in\Sigma, \tag{3.19}$$

with $0<p_i\leqslant q_i<1$. In the case of a finite number of generators $\{h_0^{-1},h_1^{-1},\ldots,h_m^{-1}\}$ each satisfying (3.19) and the sets $\Sigma_n^{i_1i_2\ldots i_n}$ being disjoint, lower and upper bounds $y_m$ and $z_m$, respectively, can be calculated for the Hausdorff dimension $\dim_H\Sigma$. These are given by the solutions to [8]

$$\sum_{i=0}^{m}p_i^{y_m}=\sum_{i=0}^{m}q_i^{z_m}=1. \tag{3.20}$$

We will consider $r=r_{\rm cr}$ only, for which

$$p_i=\frac{1}{3(i+2-1/\sqrt{3})^2}, \tag{3.21a}$$

$$q_i=\frac{1}{3(i+1)^2}. \tag{3.21b}$$

From (3.20) and (3.21), it follows that $y_m$ and $z_m$ are monotonically increasing in $m$ and are bounded by $1/2<y_m$, $z_m<1$. (Monotonicity follows from $0<p_i\leqslant q_i<1$; for $y_m$, $z_m=1/2$, the series (3.20) diverge in the limit $m\to\infty$, while for $y_m$, $z_m=1$, the series are less than one as can be readily checked.) The limit $m\to\infty$ exists for both bounds and these are the lower and upper bounds on the Hausdorff dimension

in the limit $m \to \infty$. A numerical summation of the series (3.20) for $r = r_{cr}$ gives $0.72 < \dim_H \Sigma < 0.79$.

A similar analysis can be carried out for $r < r_{cr}$. In this case, the series (3.20) become asymptotically geometrically decaying and thus converge rapidly. Solutions to (3.20) exist for all $m$ with $0 < y_m, z_m < 1$. Numerical estimates for $y_\infty$ and $z_\infty$ show that the Hausdorff dimension decreases as $r \to 0$, which is what one might expect, since the mappings $h_i^{-1}$ become more and more contracting in this limit.

In summary, we have shown that for $r \leqslant r_{cr}$, there do indeed exist initial conditions $(s_0, d_0)$ for which the trajectories generated never collapse into a corner. Moreover, whether an initial condition produces such a trajectory depends entirely on $s_0$ and is independent of $d_0$. These initial conditions for noncollapsing trajectories lie on a fractal whose dimension we estimated for $r = r_{cr}$.

## IV. CONCLUSION

We have shown that the dynamics of three inelastically colliding particles on a circle can be treated as a billiard moving in an equilateral triangle with nonspecular reflections, thereby reducing the dynamics to a discontinuous mapping of two variables. This procedure is in essence a formulation of the equations of motion in a way manifestly invariant under Galilean transformations and the simultaneous rescaling of all velocities. Its main advantage is that it enables us to uncover regularities in the asymptotic dynamics that are otherwise difficult to observe. If the dynamical variables are taken to be absolute or relative velocities, patterns can be masked by the fact that their magnitudes all decrease with each inelastic collision. Thus while it is certainly true that in the long time limit, the energy will be dissipated from the system whenever $r \neq 1$, this paper has shown that there exists a wide variety of ways in which this limit is approached.

We have examined two separate regimes in which such dissipation occurs: the quasielastic case $(1 > r > r_{cr})$ and the strongly inelastic region $(r \leqslant r_{cr})$. In the latter regime, two distinct types of asymptotic behavior emerged: inelastic collapse, where the number of collisions per unit time becomes infinite while the particles' relative separations go to zero, and, alternatively, a nonclustering state in which the separations remain finite and the mean time between collisions goes to infinity [9]. In both cases, the total energy in the center of momentum frame goes to zero; however, in the clustering state for $r < r_{cr}$, this energy is dissipated in a finite amount of time. We found that which asymptotic behavior is selected depends only on the initial ratio of relative velocities and is independent of the initial separations. The set of values of this ratio for which the particles do not cluster is fractal, and we have calculated bounds on its dimension for the special case $r = r_{cr}$.

The other regime in which energy is dissipated is $r \in (r_{cr}, 1)$. While the above results were analytic, here we mainly used computational techniques to obtain a description of the long-term dynamics of the system. We saw the emergence of pseudoperiodic trajectories in certain regions of this range of $r$ values. These orbits only visit select regions of phase space and correspond to trajectories that undergo a fixed number of reflections between each corner change. The locations (in $r$) of these windows seem to be connected to the $r$ values at which the number of reflections allowed per corner increases by one. Since the dynamics within a corner is equivalent to that of three particles on a line, these transitional $r$ values can be calculated analytically [1]. The resulting sequence of $r$'s (2.1) is countably infinite, and thus we believe that there are a corresponding number of $r$ regions in $(r_{cr}, 1)$ for which the trajectories are pseudoperiodic. We studied in some detail the orbit that goes with the first such window, $r \in (\sim 0.73, 1)$. Because of the regularity of the trajectory, we were able to do analytic work to support the numerical observations within this $r$ region.

The close examination of this nearly elastic regime allowed us to focus on the transition between energy conservation and dissipation. We found that the asymptotic behavior of perfectly elastic collisions and nearly elastic collisions in the limit of the inelasticity becoming arbitrarily small is sharply different. The main reason for this is that in the former case, the dynamics is essentially one dimensional; the motion is generated by a shift map on the unit interval and thus has zero Lyapunov exponent. In the latter case, the presence of inelasticity produces stretching and contracting in phase space and the dynamics is now two dimensional. Interestingly enough, when the collisions are sufficiently inelastic $(r \leqslant r_{cr})$, we again recover one-dimensional dynamics.

## ACKNOWLEDGMENTS

We would like to thank Peter Constantin, Amy Kolan, Mike Brenner, and Leo Kadanoff for numerous stimulating and encouraging discussions. This work was primarily supported by the MRSEC program of the National Science Foundation under Contract No. DMR-9400379.

[1] P. Constantin, E. Grossman, and M. Mungan, Physica D **83**, 409 (1995).
[2] B. Bernu and R. Mazighi, J. Phys. A **23**, 5745 (1990).
[3] S. MacNamara and W. R. Young, Phys. Fluids A **4**, 496 (1992).
[4] I. Goldhirsch and G. Zanetti, Phys. Rev. Lett. **70**, 1619 (1993).
[5] S. MacNamara and W. R. Young, Phys. Rev. E **50**, R28 (1994).
[6] E. Clement, S. Luding, A. Blumen, J. Rajchenbach, and J. Duran, Int. J. Mod. Phys. B **7**, 1807 (1993).
[7] This result was not written out in full in [1]. Equation (4.9) in [1] and the discussion following it show that the maximum number of collisions changes whenever $\pi/\phi(r)$ is an integer, with $\phi(r)$ as in Eq. (4.8). Imposing $\pi/\phi(r) = n$ and solving for $r$ using (3.7), Eq. (2.1) of this paper follows.
[8] K. Falconer, *Fractal Geometry* (Wiley, Chichester, 1990).
[9] That the separations remain finite is a consequence of the fact that a noncollapsing trajectory must keep changing corners.

Thus all possible collisions—particle 1 with particle 2, 2 with 3, and 3 with 1—continue to occur. Since the sum of the relative separations equals the circumference of the circle ($d_{12}+d_{23}+d_{31}=1$), there must always be at least one distance of order one. Since the collisions are inelastic, the absolute values of the particle velocities go to zero in the center of the momentum frame, while the distances remain finite, thus the time between collisions diverges.